Full Length Article

Formation of a cerium conversion coating on magnesium alloy using ascorbic acid as additive. Characterisation and anticorrosive properties of the formed films

A.P. Loperena, I.L. Lehr *, S.B. Saidman.

Instituto de Ingeniería Electroquímica y Corrosión (INIEC), Departamento de Ingeniería Química, Universidad Nacional del Sur, Av. Alem 1253, 8000 Bahía Blanca, Argentina

Abstract

Cerium-based conversion coatings were formed on AZ91D magnesium alloy by immersion of the substrate in solutions containing $Ce(NO_3)_3$, H_2O_2 and ascorbic acid (HAsc). The characterisation of the films was performed by electrochemical and surface analysis techniques such as SEM, EDS, X-ray diffraction and X-ray photoelectron spectroscopy (XPS). The degree of corrosion protection achieved was evaluated in simulated physiological solution by the open circuit potential monitoring, polarisation techniques and electrochemical impedance spectroscopy (EIS).

The presence of HAsc in the conversion solution causes changes in the morphology, adherence and anticorrosive performance of the films. The improvement in the corrosion resistance is closely associated with the corrosion inhibition properties of HAsc.

1. Introduction

Biodegradable metallic materials have been extensively studied in recent years due to their use in substitution and generation of tissues. Among others, magnesium appears as a very promising biomaterial [1]. Magnesium and magnesium alloys possess many excellent properties such as biocompatibility, low density and biodegradability, making them ideal candidates for implant biomaterials. Temporary implants of biodegradable materials are destined to corrode and dissolve postoperatively, hence they provide the advantage to avoiding a second surgery for implant removal [2].

However, magnesium and its alloys present a poor corrosion resistance in physiological solution and their degradation produces a layer of corrosion products mainly composed of magnesium hydroxide. Simultaneously, the hydrogen release reaction is produced. This corrosion process makes magnesium alloys subject to lose their mechanical properties in the physiological environment, a problem that needs to be settled to use the material in the biomedical field [3,4].

To improve the corrosion resistance different electrochemical treatments were investigated [5]. Among these, conversion processes are known for their low cost and simplicity of operation [6,7]. In the latest years lanthanide conversion coatings on magnesium alloys have been intensively studied because they are an environmental friendly technology. There is a lot of research about the use of cerium on conversion coatings in order to improve the corrosion resistance of magnesium biodegradable implants in physiological solution. Several studies showed that the presence of additives in a cerium conversion solution or a pre-treatment process improves the corrosion resistance of Mg alloy [8–11]. Moreover, there is no evidence that cerium compounds pose a health hazard to humans. Cui et al. reported that a cerium conversion coating acts as a protective film against corrosion of magnesium degradable implants in Hanks solution during 24 hours [9]. The coating contains trivalent and tetravalent cerium oxides. The effect of different cerium salts on the conversion treatment on AZ31 alloys was reported by Montemor et al. [10]. All coatings significantly reduce the corrosion rate of AZ31 alloys in chloride media.

* Corresponding author. Instituto de Ingeniería Electroquímica y Corrosión (INIEC), Departamento de Ingeniería Química, Universidad Nacional del Sur, Av. Alem 1253, 8000 Bahía Blanca, Argentina. Fax: +54 291 4595182.

E-mail address: ilehr@uns.edu.ar (I.L. Lehr).

Some researchers showed that better corrosion protection may be obtained by using electrochemical treatment methods. Wang and Sun reported that a uniform and protective cerium based coating can be prepared by a cathodic electrochemical technique on AZ91D magnesium alloy [11].

The formation of a conversion coating by simple immersion involves several steps, including the corrosion of the substrate, the mass transport in the liquid–substrate interface and the coating formation. The die-cast AZ91D alloy generally consists of primary α phase and eutectic α/β phase, in which β phase (intermetallic $Mg_{17}Al_{12}$) is a second phase [12]. Generally, the β phase is chemically nobler than the α phase [13]. The reduction potentials of the α and β phases are different (−1.71 V vs SHE and −1.0 V vs SHE, respectively), which leads to galvanic corrosion between the α and β phases [14,15]. The AZ91D alloy immersed in a conversion solution displays a selective dissolution which is attributed to the inherent properties of the constituent phases. In this way, the mechanism of formation of the conversion coating depends strongly on the composition and microstructure of the Mg alloy. Moreover, the dissolution behavior of the AZ91D alloy may strongly depend on the pH of the solution [16].

The main objective of the present study was to obtain cerium based conversion coatings on AZ91D magnesium alloy by a potentiostatic technique. Optimal experimental conditions were determined to obtain films with improved corrosion protection properties in simulated physiological solution. The influence of the composition of the conversion solution was analysed on both, coating formation and anticorrosive performance in simulated physiological solution.

2. Experimental procedures

The working electrodes were prepared from rods of AZ91D magnesium alloy (composition: 8.978% Al, 0.6172% Zn, 0.2373% Mn, 0.2987% Si, 0.1189% Cu, 0.00256% Ni, 0.0176% Fe, 0.00164% Ca, 0.01154% Zr, balance Mg). The rods were embedded in a Teflon holder with an exposed area of 0.070 cm^2. Before each experiment, the exposed surfaces were polished to a 1000 grit finish using SiC, then degreased with acetone and washed with triply distilled water. Following this pretreatment, the electrode was immediately transferred to the electrochemical cell. All the potentials were measured against a saturated Ag/AgCl and a platinum sheet was used as a counter electrode. The cell was a 20 cm^3 Metrohm measuring cell.

The electrodes were treated in an electrolyte solution containing cerium nitrate hexahydrate $Ce(NO_3)_3.6H_2O$ (5–50 mM) in a purified nitrogen gas saturated atmosphere. The temperature employed was 50 °C. Hydrogen peroxide (H_2O_2) and ascorbic acid (HAsc) concentrations were varied between 1–20 mM and 1–10 mM, respectively. All chemicals were reagent grade and solutions were made in twice distilled water.

Electrochemical measurements were done using a potentiostat–galvanostat PAR Model 273A and VoltaLab40 Potentiostat PGZ301. The frequency used for the impedance measurements was changed from 100 kHz to 10 mHz, and the signal amplitude was 10 mV. A dual stage ISI DS 130 SEM and

an EDAX 9600 quantitative energy dispersive X-ray analyser were used to examine the electrode surface. X-ray diffraction analysis was carried out using a Rigaku X-ray diffractometer (model Dmax III-C) with Cu Kα radiation and a graphite monochromator. X-ray photoelectron spectroscopy (XPS) has been measured in a Specs setup operatingsystem. The XPS analysis chamber is equipped with a dual anode (Al/Mg) X-ray source and a 150 mm hemispherical electron energy analyser (PHOIBOS). The analyser operated in fixed analyser transmission (FAT) mode with pass energy of 30 eV. The energies of all spectra were referenced to the C 1s peak at 285.0 eV. All the XPS spectra were deconvoluted using the CASA XPS software with a Gaussian–Lorentzian mix function.

Electrical conductivity was measured by the two-probe method using a homemade device and film adhesion was tested measuring the force necessary to peel-off the film using a Scotch® MagicTM double coated Tape 810 (3M) and a Mecmesin basic force gauge (BFG 50N).

The corrosion performance was investigated in Ringer solution at 37 °C by a potentiodynamic method, the variation of the open circuit potential (OCP) as a function of time and electrochemical impedance spectroscopy (EIS). The electrodes were allowed to equilibrate at a fixed voltage before the ac measurements. The composition of Ringer solution is (per 1 L) 8.60 g NaCl, 0.30 g KCl and 0.32 g $CaCl_2.2H_2O$.

Tafel tests were carried out by polarising from cathodic to anodic potentials with respect to the open circuit potential at 0.001 Vs^{-1} in Ringer solution. Estimation of corrosion parameters was realised by the Tafel extrapolation method. The extrapolation of anodic and/or cathodic lines for charge transfer controlled reactions gives the corrosion current density (i_{corr}) at the corrosion potential (E_{corr}). All experiments were conducted after the steady-state E_{corr} was attained, which normally took 1 h after immersion in the solution.

Each set of experiments was repeated two to four times to ensure reproducibility.

3. Results and discussion

3.1. Coating formation

In order to obtain an effectively protective cerium coating, it is essential to determine the optimal conversion parameters including the applied potential, pH of the solution and immersion time. The performance of the samples treated in different cerium-based baths was evaluated by potentiodynamic polarisation measurements in Ringer solution at 37 °C, as will be shown later. Thus, the best formation conditions were established.

A discontinuous and not adherent white coating was obtained on AZ91D alloy after immersion in a 50 mM $Ce(NO_3)_3$ solution pH 4.7 at 50 °C during 30 min under open circuit potential conditions. In order to check the effects of polarisation, different potentials were applied to the working electrode employing the same electrolyte solution. The polarisation curves in Ringer solution for the alloy covered with cerium coatings synthesised at different potentials are presented in Fig. 1. The curve for the bare alloy is also presented
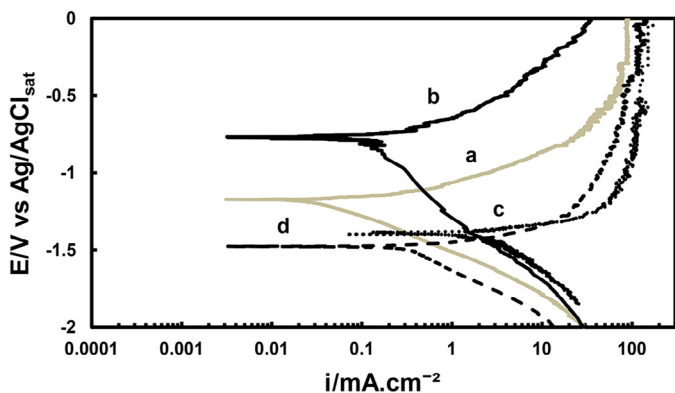
Fig. 1. Polarisation behavior in Ringer solution at 37 °C for RCe coating. The scan rate was 0.001 Vs⁻¹. The films were electrosynthesised during 30 min in 50 mM Ce(NO₃)₃ at: (a) −0.60 V, (b) −0.75 V and (c) −0.90 V. For comparison the polarisation behavior of bare alloy in Ringer is presented (curve d).

for comparison (Fig. 1, curve d). An active dissolution process of the substrate is observed starting at −1.478 V. This process is retarded when the coatings are formed on the bare alloy. It is evident that film formed at −0.75 V shows the best improvement in corrosion resistance (Fig. 1, curve b). The corresponding curve exhibits the lowest current densities, indicating that the corrosion reaction of AZ91D alloy is retarded by the presence of the coating. Thus, this potential was selected for further experiments.

Curve a in Fig. 2 shows the transient obtained for AZ91D magnesium alloy in a 50 mM Ce(NO₃)₃ solution at −0.75 V. Uniform coatings were obtained on the AZ91D alloy in solutions containing 50 mM Ce(NO₃)₃. The current decreases continually until a constant value is reached. After 30 min of immersion, the electrode was completely covered by a uniform white film. For simplicity purposes this film will be called RCe-coating.

The use of additives in the treatment solution could improve the anticorrosive performance of the RCe films. First, the effect of an oxidant in the cerium coating formation was evaluated by the addition of different hydrogen peroxide concentrations
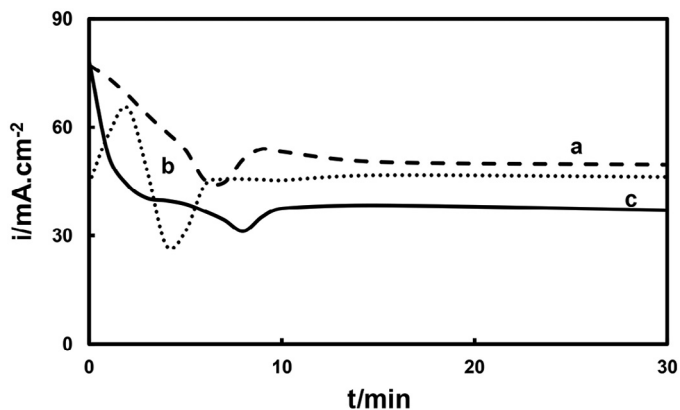
(1–20 mM). The best film was obtained for the conversion solution containing 50 mM Ce(NO₃)₃, 6 mM H₂O₂, pH 3.6. This additive produces the oxidation of Ce^{3+} to Ce^{4+} favoring the incorporation of cerium (IV) in the film [17]. As shown in Fig. 2, curve b, after reaching a maximum, the current density decreases slightly and a steady-state current density is achieved. At the end of the procedure, the substrate is coated by a yellow film. This coating will be called RCe-H₂O₂. According to the literature, cerium (IV) is responsible for the appearance of the yellow coating [18] while the presence of Ce₂O₃ or Ce(OH)₃ is related to the white color.

As was mentioned in the introduction, when the AZ91D alloy is immersed in a solution containing Ce(NO₃)₃ and H₂O₂, Mg and Al are immediately dissolved. In fact the stable species of Mg and Al are Mg^{2+} (solution pH < 8.5) and Al^{3+} (solution pH < 4), respectively [16]. This dissolution is accompanied by the proton reduction reaction and the chemical reduction of H₂O₂. It is well known that the H₂O₂ is a strong oxidising agent, and its presence in the cerium solution can promote the oxidation which accelerates the precipitation of the conversion coating. On the other hand, the presence of H₂O₂ can produce the oxidation of Ce(III) to Ce(IV). The hydrogen discharge causes a pH increase in the interface between the alloy and the solution, which promotes the reaction of the Ce(III) and Ce(IV) species with OH⁻ to form insoluble salts of Ce(OH)₃ and Ce(OH)₄ as coating components. However, Zhang et al. reported that, when the concentration of H₂O₂ is at a relatively high level, around 80 mg/L, the deposition rate of insoluble salts is increased, and in consequence, the formation of a porous coating on the metal surface occurs [17]. Thus, the addition of an appropriate amount of H₂O₂ in the conversion solution improved the corrosion resistance of Ce-based coating on AZ91D alloys.

The role of HAsc as additive was also investigated. The acid is a well-known inhibitor for several metallic materials. First, the inhibition effect of HAsc on the corrosion of bare AZ91D alloy was evaluated in Ringer solution containing different HAsc concentrations. The polarisation curves are presented in Fig. 3. It can be observed that the degradation rate of AZ91 D

Fig. 2. Potentiostatic transients obtained for AZ91D magnesium alloy at −0.75 V for 30 min in 50 mM Ce(NO₃)₃ containing: (a) 0 mM H₂O₂ and 0 mM HAsc, (b) 6 mM H₂O₂ and 0 mM HAsc and (c) 6 mM H₂O₂ and 5 mM HAsc.
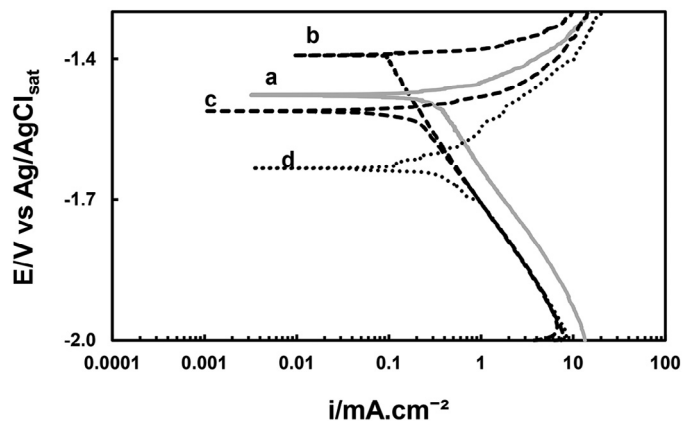

Fig. 3. Polarisation behavior for AZ91D alloy at 37 °C in Ringer solution containing: (a) 1 mM HAsc, (b) 5 mM HAsc and (c) 10 mM HAsc. The scan rate was 0.001 Vs⁻¹.

alloy is retarded by the presence of the HAsc at concentrations up to 5 mM, while the effect is opposite for higher concentrations. Thus, the best inhibitive performance was obtained for 5 mM HAsc (Fig. 3, curve b).

In order to improve the corrosion resistance of RCe-H_2O_2 coatings different HAsc concentrations were added to the conversion solution. The results in this case also show that 5 mM HAsc is the optimal concentration to use in the conversion coating formation. When this amount of HAsc is added in the solution containing 50 mM Ce(NO_3)$_3$ and 6 mM H_2O_2, and the working electrode was polarised at −0.75 V, the current decreases continually until a constant value is reached (Fig. 2, curve c). The charge involved in the transient response is lower compared to the other coatings evaluated, indicating a decrease in the rate of substrate dissolution during polarisation. At the end of the potentiostatic procedure, a golden-yellow-color was observed with the naked eyes. This film will be called RCe-HAsc.

It is known that compounds with functional groups containing oxygen act as effective inhibitors for the protection of metallic materials against corrosion in aqueous chloride solution by a surface complex formation [19]. The inhibitor character of HAsc has been extensively studied for steel in acid and neutral media [20–22]. Valek et al. reported that the formation of an oxide film on steel is associated with the inhibitive properties of HAsc due to the formation of an insoluble surface chelate at an optimal concentration of 10^{-3} M [22]. However, these authors also informed that the formation of a soluble chelate has a stimulatory action in the Fe dissolution at concentrations above 5×10^{-3} M. Pavlovic et al. also reported that HAsc exhibits a dual behavior, in some cases, it acts as corrosion inhibitor and, in other situations, the HAsc can accelerate the corrosion rate of stainless-steel (SS)X4Cr13 in HCl solutions [23]. There are currently no data in the literature about the effect of HAsc on magnesium alloys. However, the results presented above show a similar trend to that reported in the literature for other metallic materials. Thus, at an optimal HAsc concentration of 5 mM, the formation of an insoluble surface chelate provides protection to the magnesium alloy through the formation of a physical barrier. Above this optimal concentration, the degradation rate of AZ91D alloy increases probably associated with the formation of soluble chelates.

The formed RCe coatings are very adherent and could be removed only by mechanical polishing. Adhesion of the films increases when the additive is added, as can be seen from the results shown in Table 1.

Table 1
Adherence force obtained for different RCE coatings after peel-off testing. The coatings were electrosynthesised at −0.75 V during 30 min in 50 mM Ce(NO_3)$_3$, 6 mM H_2O_2 and 5 mM HAsc.

Sample	F/N
RCe	25.6
RCe-H_2O_2	34.3
RCe-HAsc	43.4

3.2. Morphology and composition of RCe-HAsc coating

After the deposition process, yellowish RCe-H_2O_2 and RCe-HAsc coatings were obtained on the AZ91D alloy. Fig. 4 shows the SEM micrograph of the coating formed in 50 mM Ce(NO_3)$_3$ + 6 mM H_2O_2 (Fig. 4A) and 50 mM Ce(NO_3)$_3$ + 6 mM H_2O_2 + 5 mM HAsc (Fig. 4B). The morphology of the first film is characterised by a cracked mud morphology. The cracks may be due to the dehydration of the surface film after the treatment [24]. In the same way, Hamlaoui et al. proposed that the cracked area is associated with the formation of gas bubbles on the substrate, combined with a dehydration process or also with shearing stresses between the alloys and the formed coating [25].

The addition of HAsc results in a more uniform and compact film with the presence of some microcracks. According to the SEM cross-sectional image of the RCe-HAsc coating, the thickness of the film is around 5 μm (Fig. 5). EDX analysis confirms the presence of cerium in the film (Fig. 6). As was
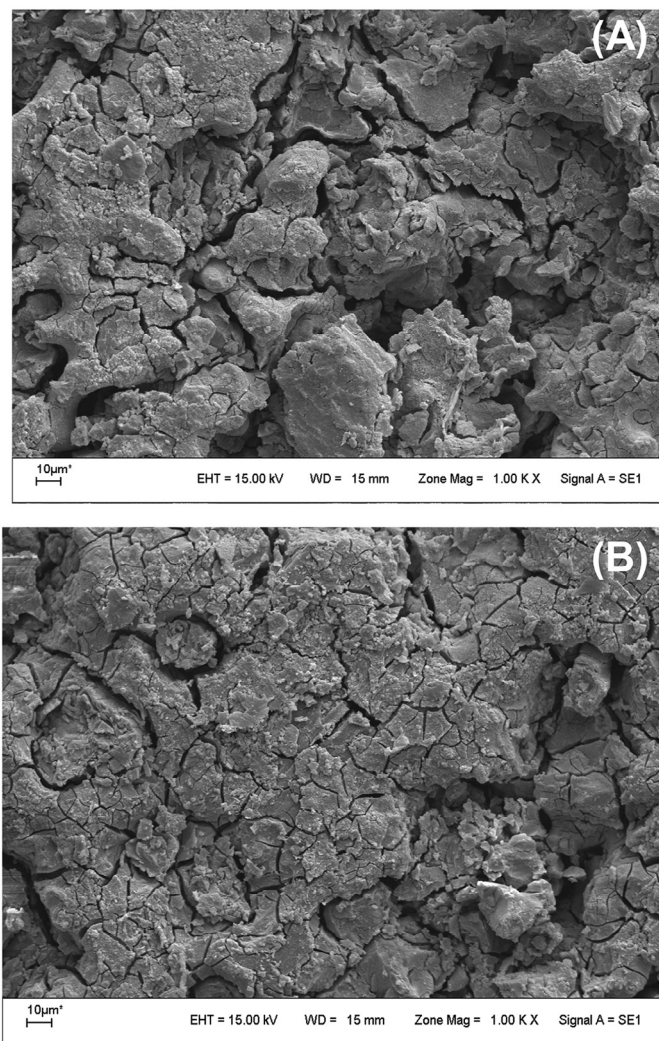

Fig. 4. SEM micrograph of the coatings formed on AZ91D alloy. The coating was electrosynthesised at −0.75 V during 30 min in a solution containing 50 mM Ce(NO_3)$_3$ and 6 mM H_2O_2: (A) without HAsc and (B) with 5 mM HAsc.
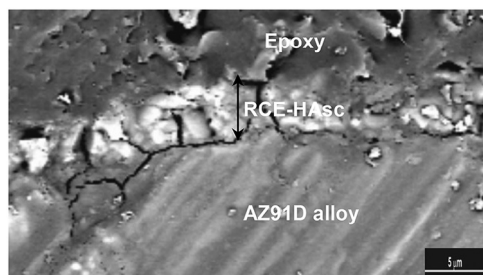
Fig. 5. SEM micrograph showing the cross-section of RCe-HAsc coating. The coating was electrosynthesised at −0.75 V during 30 min in a solution containing 50 mM Ce(NO₃)₃, 6 mM H₂O₂ and 5 mM HAsc.

Fig. 7. XRD spectra for: (a) AZ91D alloy, (b) RCe coating, (c) RCe-H₂O₂ film and (d) RCe-HAsc coating.

mentioned previously, the RCe films are formed from the precipitation of oxides, due to an increase in local pH at the interface substrate/solution.

By comparing the XRD patterns of the treated samples with that of the untreated one it can be concluded that the coatings are composed of CeO_2, Ce_2O_3 and $Mg(OH)_2$ (Fig. 7).

XPS was employed to determine the surface chemical composition of RCe-HAsc coating. The XPS results are shown in Fig. 8. Magnesium, oxygen and cerium are the main components. A more detailed XPS analysis of the specific electron binding energies of Mg, O and Ce elements is presented (Fig. 9). The Mg 2p spectrum is displayed in Fig. 9A indicating that Mg in the coating is present as MgO and $Mg(OH)_2$ [2]. The spectrum of O 1s is presented in Fig. 9B. The peak at 531.25 eV is attributed to metallic oxides [2]. As shown in Fig. 9C, the Ce $3d_{5/2}$ and Ce $3d_{3/2}$ peaks are analysed. The results indicate that the RCe-HAsc coating is composed of a mixture of CeO_2, CeO, Ce_2O_3 and the corresponding binding energies are at 916.0 eV, 897.89 eV and 880.90 eV, respectively. The presence of Ce(IV) ions is confirmed by the satellite peak around 916.0 eV. The ratio between Ce(IV) and Ce (III) was 1.503. Summarising, based on the XPS result, it was concluded that the RCe-HAsc
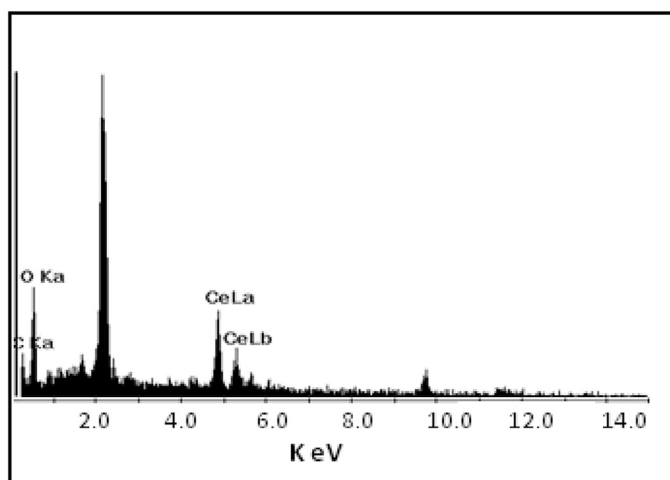
coating is mainly composed of CeO_2, CeO, Ce_2O_3, MgO and $Mg(OH)_2$.

3.3. Evaluation of the anticorrosive properties of the coatings

Fig. 10 shows the variation of the open circuit potential (OCP) as a function of time in Ringer solution at 37 °C. This method allows to evaluate the degree of corrosion protection attained after covering the substrate. When the coating is not sufficiently protective the pitting potential of the uncovered electrode (−1.503 V) is inevitably reached (Fig. 10, curve a). The initial OCP value for RCe-HAsc was −1.32 V (Fig. 10, curve d). Then, the OCP increases until around −1.15 V where it remains for approximately 18 h. After 72 h of immersion, the OCP value is approximately −1.35 V. This potential value was still nobler than that for the uncoated electrode. The corrosion potential of the uncoated AZ91D alloy is reached faster for the other coatings (Fig. 10, curves b and c).

In order to confirm the improvement in the corrosion protection of the AZ91D alloy, after the OCP measurements, the electrolyte solutions were analysed to determine the concentration of released ions from the samples. The quantity of Mg
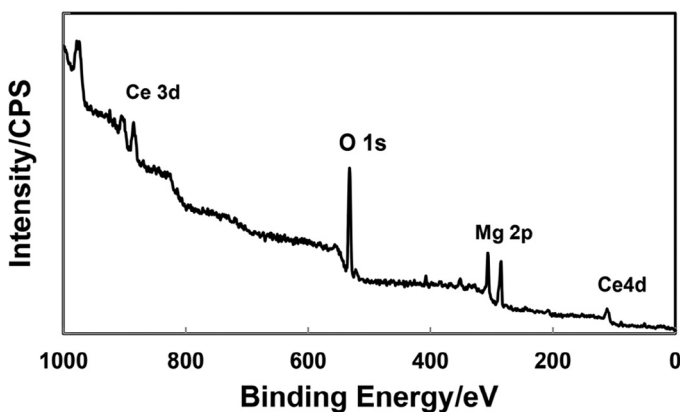

Fig. 6. EDS spectrum of RCe-HAsc coating formed on AZ91D alloy. The coating was electrosynthesised at −0.75 V during 30 min in a solution containing 50 mM Ce(NO₃)₃, 6 mM H₂O₂ and 5 mM HAsc.

Fig. 8. XPS survey spectrum of RCe-HAsc coating formed on AZ91D alloy. The coating was electrosynthesised at −0.75 V during 30 min in 50 mM Ce(NO₃)₃, 6 mM H₂O₂ and 5 mM HAsc.
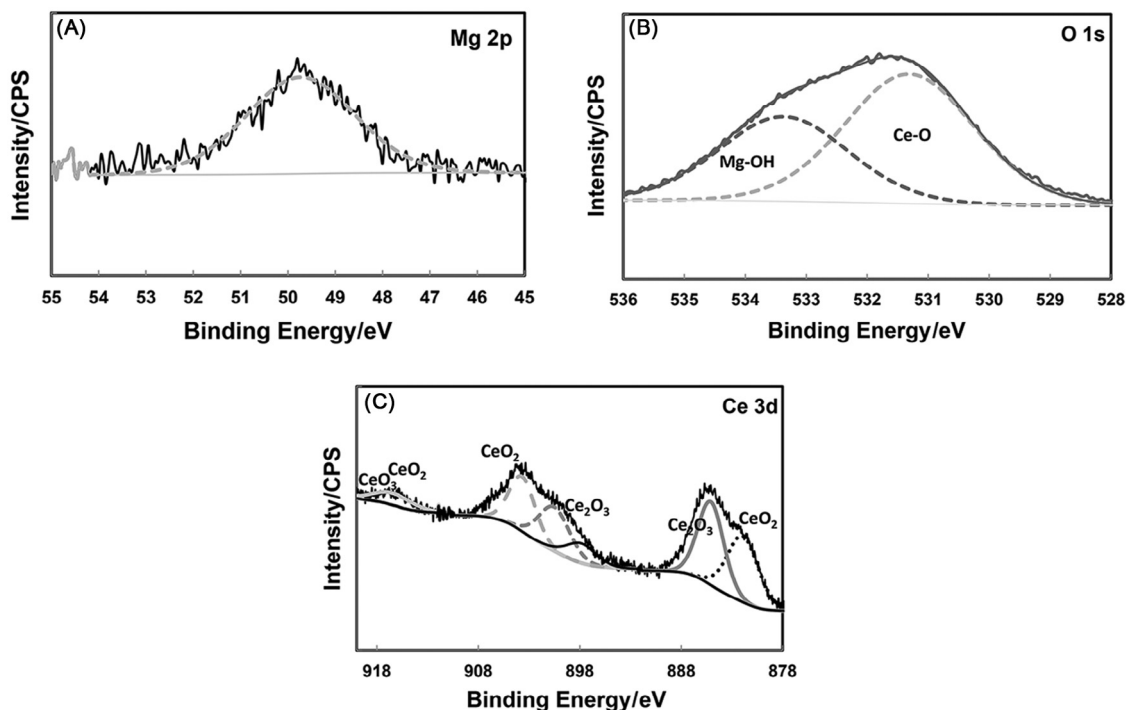
Fig. 9. XPS intensities of: (A) Mg 2p, (B) O 1s and (C) Ce 3d. The coating was electrosynthesised at −0.75 V during 30 min in 50 mM $Ce(NO_3)_3$, 6 mM H_2O_2 and 5 mM HAsc.

released is 2.01 mg/L when the substrate was coated with the RCe-HAsc film, while a value of 3.90 mg/L was obtained for the uncoated electrode. That is, magnesium degradation rate is nearly twice less for the RCe-HAsc film. This result confirms a good performance of the RCe-HAsc coating even after a long exposure time.

Tafel plots for uncoated and coated AZ91D alloys are presented in Fig. 11. Estimation of the corrosion parameters (E_{corr}, cathodic (B_c) and anodic (B_a) Tafel slopes and corrosion current (i_{corr})) is reported in Table 2 for all coatings studied. The i_{corr} values measured for the RCe coatings are lower than that for the bare AZ91D alloy. However, this decrease is more noticeable for the RCe-HAsc films, their i_{corr} being one order of magnitude lower than that of the uncoated substrate.
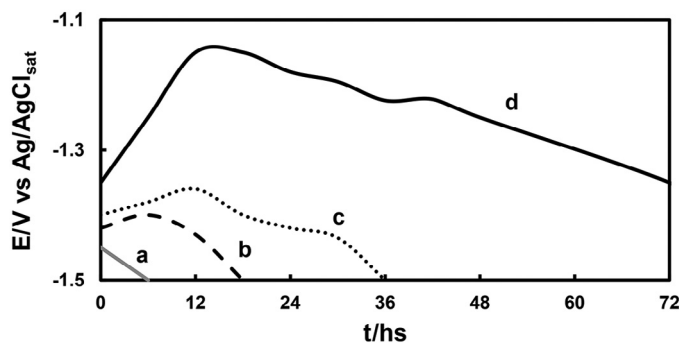
The polarisation curves in Ringer solution at 37 °C are presented in Fig. 12. By comparing them, it is evident that the coatings provide a significant improvement in the corrosion resistance. The curves initially exhibit low current densities (Fig. 12, curves b, c and d), indicating that the corrosion reaction of AZ91D alloy is retarded by the presence of the coating. In the case of the RCe-HAsc film a significative increase in the anodic current can be observed at more anodic potential values (Fig. 12, curve d).

EIS measurements were conducted to evaluate the anticorrosive performance of RCe-HAsc coating at different immersion
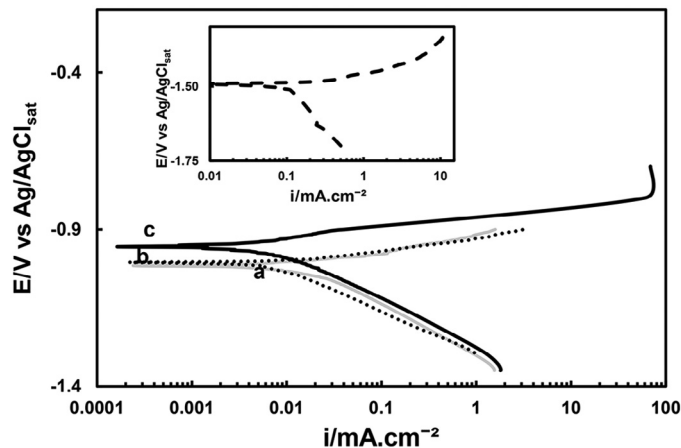

Fig. 10. Time dependence of the OCP in Ringer solution for: (a) AZ91D magnesium alloy, (b) RCe coating, (c) RCe-H_2O_2 film and (d) RCe-HAsc coating.

Fig. 11. Tafel curves obtained in Ringer solution at 37 °C for different coatings: (a) RCe, (b) RCe-H_2O_2 and (c) RCe-HAsc. For comparison the curve of uncoated AZ91D alloy is presented (small insert). The scan rate was 0.001 Vs^{-1}.

Table 2
Corrosion parameters calculated from Tafel polarisation plots for uncoated AZ91D, RCe-H$_2$O$_2$ and RCe-HAsc formed on AZ91D alloy. The mean values and their standard deviation are presented.

	E_{corr}/V	i_{corr}/mAcm^{-2}	B$_a$/V	B$_c$/V
AZ91D	−1.501 ± 0.050	0.1050 ± 0.0050	0.045	−0.293
RCe	−1.021 ± 0.020	0.0198 ± 0.0005	0.052	−0.141
RCe-H$_2$O$_2$	−1.002 ± 0.020	0.0057 ± 0.0002	0.034	−0.122
RCe-HAsc	−0.952 ± 0.015	0.0054 ± 0.0002	0.032	−0.126

times in Ringer solution at 37 °C. The impedance spectra recorded for the AZ91 alloy after cerium, H$_2$O$_2$ and HAsc conversion treatment are shown in Fig. 13A. After 6 h of immersion, all the impedance diagrams exhibit a capacitive loop in the high and medium frequency ranges. It is known that the diameter of the capacitive loops is associated with the charge-transfer resistance (R$_{ct}$) and therefore with the corrosion resistance. For comparison, the impedance response of uncoated substrate in Ringer solution was presented in Fig. 13B. The Nyquist diagram of the uncoated sample, as most of the magnesium alloys, shows two capacitive loops and one inductive loop [26]. Some authors suggest that the inductive loop at low frequencies may be due to the existence of relaxation processes
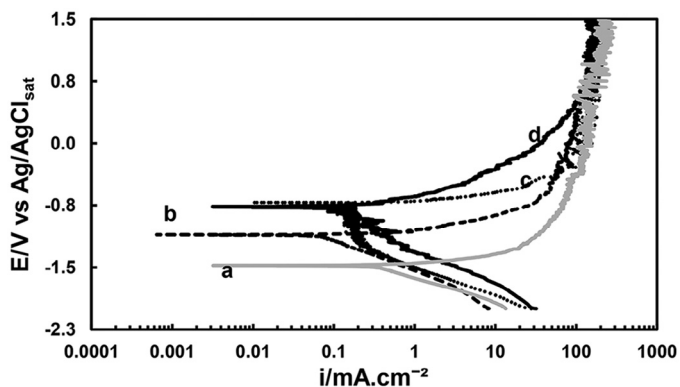

Fig. 12. Polarisation behavior in Ringer solution at 37 °C for: (a) uncoated AZ91D alloy, (b) RCe film, (c) RCe-H$_2$O$_2$ coating and (d) RCe-HAsc coating. The scan rate was 0.001 Vs^{-1}.

of adsorbed species on the electrode surface (Mg(OH)$^+$ or Mg(OH)$_2$) for untreated alloys/pure Mg [27]. The R$_{ct}$ values for RCe-HAsc coatings are much larger than that of the untreated electrode indicating a corrosion protection (Fig. 13A). The increase in the total impedance was attributed to the presence of RCe-HAsc film, which acts as a physical barrier between the substrate and the corrosive medium.

The uncoated AZ91D alloy suffers serious corrosion in a simulated body fluid solution. As was already stated, it is postulated that the general corrosion mechanism of Mg alloys involves Mg oxidation to Mg^{2+} with simultaneous water reduction, and later, the precipitation of Mg(OH)$_2$ due to the local alkalisation produced by cathodic reactions [28,29]. The α-phase acts as the anode and the β-phase as the cathode. The RCe-HAsc coating reduces the active surface area, and less area of the alloy is available to be corroded. When the substrate is covered by an adherent and stable coating, the potential difference between α and β phases becomes smaller and the micro-galvanic couple effect is reduced [14,15]. Thus, the film provides a physical barrier between the substrate and the corrosive medium. Moreover, the addition of ascorbic acid increases significantly the anticorrosive properties of these coatings. As mentioned previously, this improvement in the corrosion resistance could be associated to the HAsc inhibition ability by insoluble chelates formation. The presence of HAsc decreases the dissolution rate of the substrate during the coating formation allowing the formation of a more compact and protective film.

4. Conclusions

Adherent and uniform RCe-HAsc coatings were obtained on AZ91D magnesium alloy in solutions containing cerium nitrate, H$_2$O$_2$ and HAsc. The most adherent films were obtained by a potentiostatic polarisation at −0.75 V. The coating with a thickness of approximately 5 μm is mainly composed of magnesium oxides or hydroxides and cerium oxides. The corrosion performance of RCe-HAsc film in simulated physiological solution is superior to those of films formed in the absence of HAsc. The improvement in the anticorrosive properties is associated with the inhibitor effect of the additive by insoluble chelates formation.
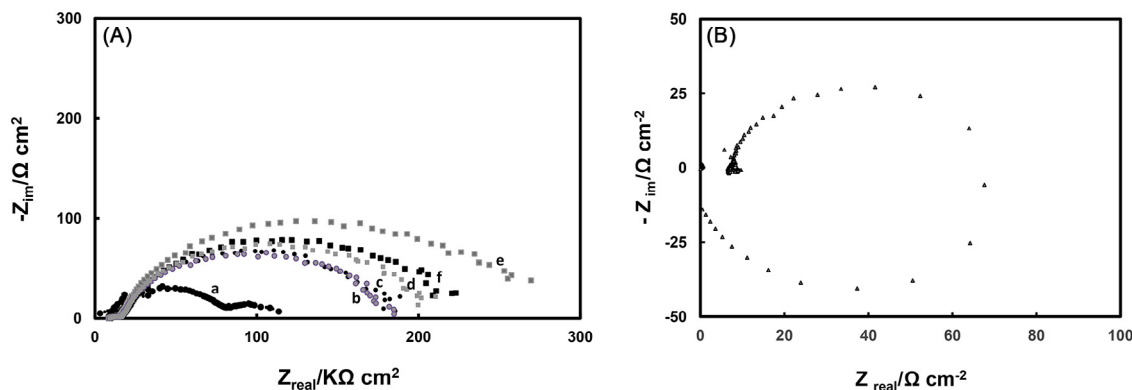

Fig. 13. Nyquist plots of the impedance spectra obtained at the open circuit potential in Ringer solution at 37 °C for: (A) RCe-HAsc coating, after different immersion times: (a) 5 min, (b) 6 h, (c) 12 h, (d) 24 h, (e) 36 h and (f) 48 h. The coating was electrosynthesised at −0.75 V during 30 min in a solution containing 50 mM Ce(NO$_3$)$_3$, 6 mM H$_2$O$_2$ and 5 mM HAsc. (B) Nyquist plot for uncoated AZ91D alloy after 5 min of immersion.

Acknowledgement

References

[1] P. Tian, X. Liu, Regen. Biomater. 2 (2015) 135–151.
[2] Y.F. Zheng, X.N. Gu, F. Witte, Mater. Sci. Eng. R Rep. 77 (2014) 1–34.
[3] A. Atrens, G. Song, F. Cao, Z. Shi, P. Bowen, J. Magnes. Alloys 1 (2013) 177–200.
[4] P. Wan, L. Tan, K. Yang, J. Mater. Sci. Technol. (2016) doi:10.1016/j.jmst.2016.05.003.
[5] X.B. Chen, N. Birbilis, T.B. Abbott, Corrosion 67 (2011) 035005-1–035005-16.
[6] Y. Chen, Z. Xu, C. Smith, J. Sankar, Acta Biomater. 10 (2014) 4561–4573.
[7] S. Pommiers, J. Fryret, A. Castetbon, M. Potin-Gautier, Corros. Sci. 84 (2014) 135–146.
[8] H. Hornberger, S. Virtanen, A.R. Boccaccini, Acta Biomater. 8 (2012) 2442–2455.
[9] X. Cui, Y. Yang, E. Liu, G. Jin, J. Zhong, Q. Li, Appl. Surf. Sci. 257 (2011) 9703–9709.
[10] M.F. Montemor, A.M. Simoes, M.G.S. Ferreira, M.J. Carmezim, Appl. Surf. Sci. 254 (2008) 1806–1814.
[11] J. Sun, G. Wang, Surf. Coat. Technol. 254 (2014) 42–48.
[12] H. Li-Fang, Q. Meng, S. Chen, H. Wang, Appl. Surf. Sci. 259 (2012) 816–823.
[13] H.Y. Yang, X.B. Chen, X.W. Guo, G.H. Wu, W.J. Ding, N. Birbilis, Appl. Surf. Sci. 258 (2012) 5472–5481.
[14] L. Pezzato, K. Brunelli, E. Napolitani, M. Magrini, M. Dabalà, Appl. Surf. Sci. 357 (2015) 1031–1039.
[15] Y.W. Song, D.Y. Shan, E.H. Han, Electrochim. Acta 53 (2008) 2135–2143.
[16] W. Zhou, D. Shan, E. Han, W. Ke, Corros. Sci. 50 (2008) 329–337.
[17] S. Chen, S. Zhang, X. Ren, S. Xu, L. Yin, Int. J. Electrochem. Sci. 10 (2015) 9073–9088.
[18] C. Wang, S. Zhu, F. Jiang, F. Wang, Corros. Sci. 51 (2009) 2916–2923.
[19] Y.I. Kuznetsov, Organic Inhibitors of Corrosion of Metals, Plenum Press, NY and London, 1996.
[20] E.S. Ferrerira, C. Giacomellu, A. Spinelli, Mater. Chem. Phys. 83 (2004) 129–134.
[21] H. Akrout, L. Bousselmi, E. Triki, S. Maximovitch, F. Dalard, J. Mater. Sci. 30 (2004) 7341–7350.
[22] L. Valek, S. Martinez, D. Mikulic, I. Brnardic, Corros. Sci. 50 (2008) 2705–2709.
[23] R. Fuchs-Godex, M. Pavlovic, M. Tomic, Int. J. Electrochem. Sci. 8 (2013) 1511–1519.
[24] K. Brunelli, M. Dabalá, J. Calliani, M. Magrini, Corros. Sci. 47 (2005) 989–1000.
[25] Y. Hamlaoui, F. Pedraza, C. Remazeilles, S. Cohendoz, C. Rébéré, L. Tifouti, et al., Mater. Chem. Phys. 113 (2009) 650–657.
[26] A. Srinivasan, C. Blawert, Y. Huang, C.L. Mendis, K.U. Kainer, N. Hort, J. Magnes. Alloy. 2 (2014) 245–256.
[27] M. Anik, G. Celikten, Corros. Sci. 49 (2007) 1878–1894.
[28] Y. Zhang, C. Yan, F. Wang, W. Li, Corros. Sci. 47 (2005) 2816–2831.
[29] A. Pardo, M.C. Merino, A.E. Coy, R. Arrabal, F. Viejo, E. Matykina, Corros. Sci. 50 (2008) 823–834.